Polarimetric dark-field spectroscopy of gold bipyramids: measuring single particle 3D orientation

Cam Nhung Vu, Zakarya Ouzit, Clotilde Lethiec, Michel Pellarin, Agnès Maitre, Frédéric Lerouge, Laurent Coolen, Julien Laverdant

Title: **Polarimetric dark-field spectroscopy of gold bipyramids: measuring single particle 3D orientation**

Cam Nhung VU[1], Zakarya OUZIT[2], Clotilde LETHIEC[2], Michel PELLARIN[1], Agnès MAITRE[2], Frédéric LEROUGE[3], Laurent COOLEN[2] AND Julien LAVERDANT [1,*]

1. Institut Lumière Matière, Université Claude Bernard Lyon 1, CNRS, Université de Lyon, F-69622 Villeurbanne, France

2. Sorbonne Université, CNRS, Institut des NanoSciences de Paris, INSP, F-75005 Paris, France

3. Univ Lyon, Ens de Lyon, CNRS, Université Lyon 1, Laboratoire de Chimie UMR 5182, F-69342, Lyon, France

*Corresponding author: Julien Laverdant, Institut Lumière Matière, Université Claude Bernard Lyon 1, CNRS, Université de Lyon, F-69622 Villeurbanne, France, Phone : +33 (0)4 72 43 11 21 , julien.laverdant@univ-lyon1.fr

Abstract:

We determine the 3D orientation of single gold nano-bipyramids (AuBPs) deposited on a glass substrate. These nanoparticles possess a well-defined localized surface plasmon resonance along their main axis which can be modeled as a single dipole. Orientation is deduced by polarization resolved dark-field scattering. For that purpose, a specific experiment has been built to select, analyze in polarization and resolve the scattering angles at the single nanoparticle level. Usually, the out-of-plane angle is deduced by measuring the degree of polarization (DOP) and doing numerical simulations taking into account the nature of the dipole (1D, 2D) and all experimental parameters. We compare this method with a complete measurement of the DOP as function of the collected numerical aperture (controlled by Fourier filtering). The results provide the accuracy of the polarimetric measurements. The complimentary method proposed in this article can easily be extended to more complex system.

Keywords:

Plasmon resonance, Optical Microscopy, Polarization, Nano-optic, Nanoparticle

1. Introduction

Recent advances in nanofabrication allowed the elaboration of metallic nanoparticles with various shapes and sizes [1-3]. Such systems present great interest due to their well-known plasmon resonance properties. Among these, nanoparticles with sharp tips are very attractive as nanoantennas either to radiate or absorb light very efficiently [4] leading to many applications such as single photons sources, nano-light sources or photocatalytic activity [5-8]. In that context, more complex systems have also been proposed such as a single nano-object inserted in a nano-cavity [9], for studying coupled effects in nanoparticles assemblies such as nanoparticle chains [10] or for improving metal enhanced fluorescence [11].

In all these devices, two parameters are critical: the position and the orientation of the nanoparticle. Usually, the localization of the nano-object is addressed through different methods such as AFM [12] or in-situ lithography [13]. Indeed, the knowledge of single nanoparticle orientation is a key parameter to tune collective effects and to couple to the desired mode [14]. Thus, the ability to measure accurately the position of a single nano-object is of great importance. So far, many optical methods have been proposed to determine the orientation of the nanoparticle. It is possible to categorize them as follow: radiation pattern, polarization analysis and other alternative methods.

Orientation measurements from the radiation pattern have been proposed such as defocused imaging and Fourier plane imaging. Although defocused imaging has been successfully used for deposited objects [15] or to track the nanoparticle "in volume" [16], this technique is somehow limited and cannot be implemented in all cases: in particular, if the nanoparticle is located close to an absorbing

surface [17]. In the case of the Fourier plane imaging, the full collected emission diagram is captured by a CCD camera and requires an intense signal and the use of a very sensitive detector [18, 30, 31]. Otherwise, polarization methods are also used to determine the 3D orientation of nanoparticles. By rotating a polarizer in the detection path, its in-plane as well as its out-of-plane angle may be retrieved [19, 20,21]. As the main difficulty is to deduce the out-of-plane angle, another method has been proposed using a phase plate to increase this particular component [22].

Alternative and more complex techniques have also been suggested for non-luminescent samples, such as photothermic imaging or methods involving local surroundings. As an example, in the case of gold nanorod, a laser was used to heat the sample by absorption at the transverse resonance (independent of the length of the nanorod) and the orientation was measured by polarization analysis [23]. Another interesting method consists in a precise measurement of the out-of plane orientation of the gold nanorod on a metallic substrate, by projecting its doughnut - shaped scattering pattern on the back foal plane of the TIR scattering microscope [24]. However, the result becomes more difficult to interpret when the hybridization of the plasmons between the nano-object and the surface appears at a very small separation.
In this paper, we will consider scattering polarization analysis. Polarimetric measurements have been successfully used to determine the 3D orientation of fluorescent molecules or quantum dots [20]. A polarizer with rotating angle α is placed on the detection pathway. The detected intensity oscillates between a maximum (I_{max}) and a minimum (I_{min}) value according to the Malus law:

$$\mathrm{I}(\alpha) = I_{min} + (I_{max} - I_{min})cos^2(\phi - \alpha). \quad \textbf{(1)}$$

The in – plane angle ϕ is retrieved when the polarization direction is parallel to the projection of dipole in the substrate plane ($\alpha = \phi$) which gives a maximum signal in transmission.

For a given numerical aperture (NA) of the collection objective, the out – of – plane angle Θ is determined by confronting the measured degree of polarization (DOP) δ obtained as:

$$\delta_{\mathrm{NA}} = \frac{I_{max} - I_{min}}{I_{max} + I_{min}}, \quad \textbf{(2)}$$

with its theoretical expression as a function of Θ. It is important to stress that numerical calculations need to account for both the nature of the emission (dipolar or multipolar) and the experimental configuration (interface and the collected numerical aperture for collection). While these environmental parameters are easily defined, the dipolar nature is difficult to be distinguished because there is a subtle quantitative difference in the $\delta_{\mathrm{NA}}(\Theta)$ curves of the 1D dipole (linear radiating) and the 2D dipole (incoherent sum of two orthogonal 1D dipoles) [17]. In other words, this relation is insufficient to measure both orientation and dipolar nature of the nanoparticles at the same time. Therefore, choosing a suitable model for fitting is the main difficulty of the polarimetric method. Some previous works combined polarization measurements with defocused imaging [25] or Fourier plane imaging [26] to address the nature of the radiation.

Recently, in a previous publication, we have demonstrated that the polarimetric measurement of 3D orientation strongly depends on the NA of the collection objective by experimentally measuring the δ at different NA [28]. In fact, from the dependence of δ(NA), the out – of – plane angle Θ can also be determined with a higher certainty in defining the dipolar nature. Therefore, the aim of the present work is to compare the two methods of Θ determination, i) extracted from the theoretical curve and the experimental value of $\delta_{\mathrm{NA}}(\Theta)$ obtained at a fixed known NA and ii) by the fitting of the experimental curve δ(NA) obtained from different numerical apertures.

In order to conduct such study, anisotropic gold particles were needed. We choose gold bipyramid nanoparticles (AuBPs) as an ideal system which can be considered as a 1D dipole [27]. Because of their sharp-end tips, AuBPs are known to act as a strongly radiating dipole when their longitudinal plasmon resonance is excited. This resonance can be tuned in the visible or in the near infra-red by increasing the nanoparticles length. We will use the theoretical model presented in [17] where the dipole is located near a planar interface delimiting two semi-infinite media.

2. Experimental set-up

The dark field imaging experimental set up is depicted in Fig.1(a). A diluted suspension of the AuBPs in water is dropped on a glass substrate. The concentration is adjusted to avoid interactions between them. The light source is provided by a fibered white lamp and focused onto the sample with an objective of low numerical aperture (NA=0.25). The light is then collected by an oil immersion objective (NA=1.49).
At the end of the objective, the beam passes through a confocal system to manipulate the Fourier plane of collection. A beam stop is inserted to effectively block the excitation beam (blocked NA 0.5). An example of a dark-field image is displayed in Fig.1(c). The polarization analysis is made by a combination of a rotating achromatic $\lambda/2$ plate and a fixed polarizer. Finally, a spectrometer is used to select single AuBP by its resonance, an example is presented Fig.1(d).

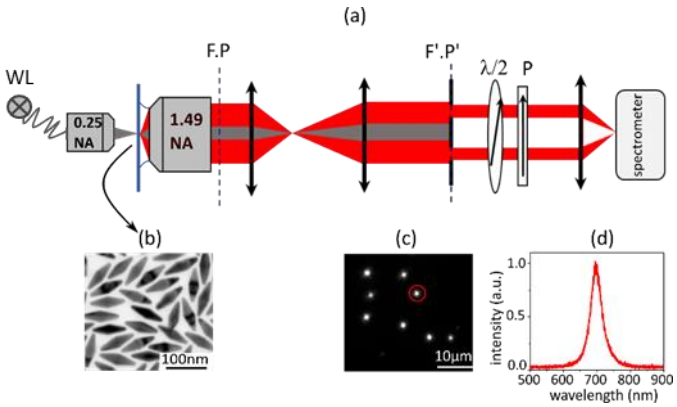

Figure. 1. (a) Schematic of the experimental set-up. WL: white lamp, F.P: Fourier Plane. F'.P': deported Fourier Plane. λ/2: half-wave plate. P: linear polarizer. (b) A TEM image of AuBPs (c) A dark-field image of the AuBPs deposited on a glass substrate. (d) Scattering spectrum of a single AuBP.

With this optical configuration, we identify a single AuBP in the dark-field by spectroscopy. The AuBPs possess a well-defined plasmon resonance around 700nm with a narrow full width at half-maximum (FWHM) of 40nm. This resonance is attributed to the plasmon longitudinal mode. When rotating the half-wave plate, the detected intensities vary with the analysis angle α, following the square-cosine function in Eq (1). The in-plane angle Φ, I_{max}, and I_{min} are extracted from the fit. At the largest collection of the objective NA = 1.49, we find a DOP $\delta_{NA=1.49}$= 0.69 for the AuBP of Fig.2. Using the theoretical calculation of $\delta_{NA=1.49}(\Theta)$ on Figure 2a [17], an out – of – plane angle $\Theta_{NA=1.49}$= 74° is deduced with an error $\widetilde{\Theta}_{NA=1.49}$ = 3° (estimated from the fit of the Malus law which gives 5% of error on the DOP).

3. Polarization measurement of single gold bipyramid with the numerical aperture

In the following, we present a second way to measure the angle Θ from the dependence of δ(NA). A diaphragm is placed at the deported Fourier plane position, F'P' in Fig.1(a), to remove the high spatial frequencies. An example is inserted in Fig.2(b). The collected scattering is then integrated for numerical apertures in the range of [0.5; NA] where the NA is defined by the opening of the diaphragm. For each diaphragm opening, from NA=0.65 (limitation by the beam stop) to 1.49 (NA of the oil objective), we repeat measurements of the DOP. The plot of δ(NA) on the same AuBP is shown on Figure 2(b). For clarity, a scheme of the controlled collection NA on the Fourier plane is also presented. As expected the degree of polarization decreases with the NA because more radiation directions are collected with different polarization orientations. By adjusting Θ in the simulations we obtain a confidence value Θ_{fit} = 70° with an error $\widetilde{\Theta}_{fit}$= 4°.

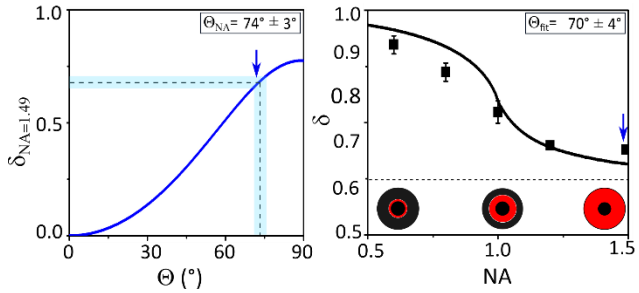

Figure. 2. Polarimetric measurement of the same isolated AuBP. (a) Theoretical evolution of the DOP δ_(NA=1.49) (Θ). The dots correspond to the experimental data and the blue area represents the error bar. (b) Evolution of δ wih the objective numerical aperture δ (NA). The line is obtained with the theoretical model. The insert represents a scheme of the Fourier plane where the black disk illustrates the total NA of the objective and the orange red corresponds to the lights collected. The blue arrows show the same measured values for NA=1.49.

On this particular example, there is a small difference in the out – of – plane angle Θ measured by the two methods that is still inside the range of the error bar. It is worth noting that in both measurements, the experimental parameters (substrate composition, thickness…) have been considered and the AuBP is modeled as a linear dipole.

We are convinced that the multiple points measurements in Fig.2(b) and their global comparison with the theory, assuming the dipolar nature of the emission, give a much more reliable information that the one that could be obtained from a single measurement at fixed NA $\delta_{fix\ NA}(\Theta)$ in Fig.2(a).

Simulations of the scattering spectrum and radiation pattern were performed with finite element methods (COMSOL, 5.2 software). The AuBP is modeled as a 100 nm long bipyramid of square basis with lateral size of 30nm. The tips are slightly truncated with a square basis of 3nm width. It was set on a glass substrate with an angle of 15° and excited by a plane wave in normal incidence (Fig.3).

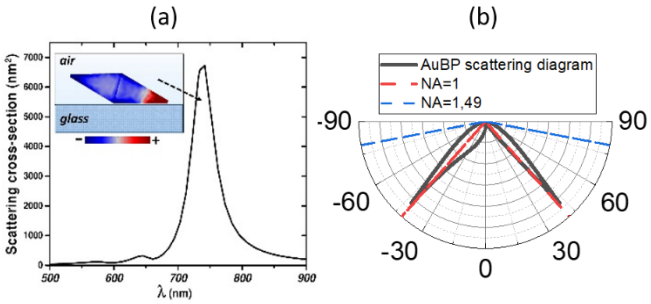

Figure 3. Numerical simulations of the AuBP optical properties. (a) Scattering spectrum together with, in insert, the charge distribution associated at the main resonance (740 nm). (b) Corresponding scattering diagram in the glass substrate. The blue dashed line represents the maximum collected angles (NA=1.49) and the red dashed line corresponds to the glass-air total internal reflection angle (NA=1).

In Fig.3(a), the simulated spectrum displays a longitudinal plasmon resonance at 740nm. The associated charge distribution simulated at this resonance displays a dipolar pattern which confirms the previous hypothesis of our polarization model (fig 3(a) insert). Furthermore, on Fig.3(b), we observe a strong modification of the radiation pattern of the particle due to the air-glass interface. At full experimental NA=1.49, we collect all the radiation emitted in the glass. We also observe a strong modification of the radiation pattern around NA=1 which corresponds to the total internal reflection angle of the glass-air interface.

4. Statistical analysis

In the following, we compare the two previous methods to determine the orientation. The procedure explained for Fig.2 was repeated with other AuBPs presenting different out – of – plane orientations (within a range 70-90° because of the AuBP geometry). For this, we calculate the relative difference between the angles obtained by the two methods as:

$$\Delta\Theta = \frac{\Theta_{\text{fit}} - \Theta_{\text{NA}}}{\Theta_{\text{fit}}} \qquad \textbf{(3)}$$

Fig.4 displays the obtained results of $\Delta\Theta$ at different NA and the error $\widetilde{\Theta}_{fit}$ is taken as a reference.

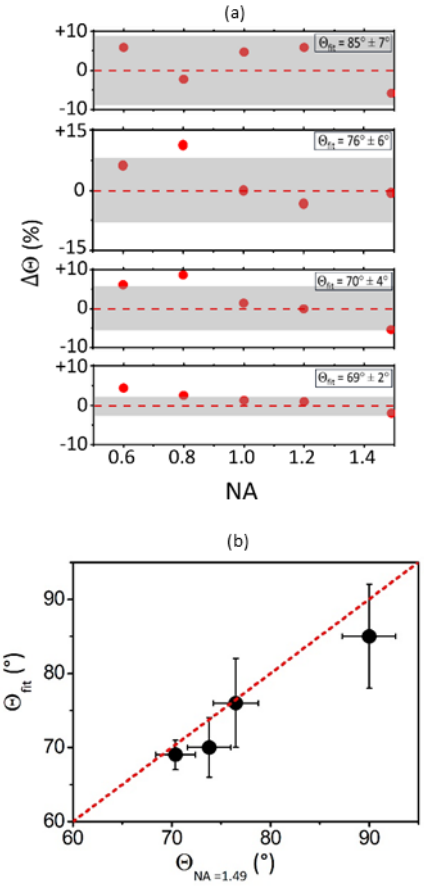

Figure 4. (a) Relative difference between Θ_{fit} and Θ_{NA} for four different AuBPs (red dots). The grey area displays the error $\widetilde{\Theta}_{\text{fit}}$. (b) Θ_{fit} as function of $\Theta_{\text{NA=1.49}}$. The dashed line represent the ideal case when $\Theta_{\text{fit}} = \Theta_{\text{NA=1.49}}$. The error bars corresponds to $\widetilde{\Theta}_{fit}$ and $\widetilde{\Theta}_{\text{NA=1.49}}$.

In Fig.4(a), we observe that the relative error $\Delta\Theta$ between each method (red dots) is included inside the error on the fitting value $\widetilde{\Theta}_{fit}$ (grey area). Especially, the relative error is weakest (the two measurements give nearly the same result) around NA=1. Indeed, the polarization behavior is directly linked to the radiation diagram [4] and when a dipole is located near a glass-air interface, most of the emission is distributed between numerical apertures of 1-1.1 which is observed in Fig3(b). This result has been observed in defocused imaging [29] where, i) for smaller NA, the collection angles do not contain enough information on the angle Θ and, ii) for higher NA, the high collection decreases the signal to noise ratio. Moreover, we also point out that the errors increase with the Θ_{fit}. Indeed, at every collection NA, the degree of polarization is nearly the same for any orientation in the range 80-90° [28]. In other words, the measurement is less sensitive when the nanoparticles are nearly positioned parallel to the substrate.
In Fig. 4(b), we present the direct comparison between both methods by plotting Θ_{fit} as function of $\Theta_{\mathrm{NA=1.49}}$. The errors of each angles ($\widetilde{\Theta}_{\mathrm{fit}}$,$\widetilde{\Theta}_{\mathrm{NA=1.49}}$) are also displayed. In accordance with the previous discussions, the values of the deduced angles by each means are very similar. The ideal case, in an absence of any deviation between each measurement, is represented by the dashed line in Fig.4(b). The relative standard deviation of our results to this ideal line is around 10% which is within the displayed error bars. Furthermore, we also note that Θ_{fit} undersestimates the values of $\Theta_{\mathrm{NA=1.49}}$. In accordance to the previous discussions, we observe more deviations for angles near 90°.

5. Conclusion

In this work, we have deduced the 3D orientation of a single gold bipyramid by polarization scattering-spectroscopy. We have paid attention more specifically to the measurement of the out-of-plane angle Θ. A comparison of two methods has been performed to deduce a more reliable value. On one hand, Θ is calculated from a measurement of the degree of polarization (DOP) and thanks to an adequate model, this angle is estimated. On the other hand, Θ is deduced from an evolution of the DOP with the numerical aperture of the objective. In the latter case, the agreement between the measured and the theoretical curves helps us to validate the proposed model. The evolution of the DOP with many different NA reinforces the validity of the extracted values even if the comparison between the two models gives similar results with a relative deviation less than 10%. We believe that the combination of Fourier filtering (control of NA) together with polarization measurement may be applied to analog nanostructures [32] or more complex systems to get new physical insights.

Funding. French Region Auvergne Rhône-Alpes, project SCUSI n°1700936601

Acknowledgment. We acknowledge the USTH French consortium that support this work.

References

[1]. C. Bréchignac, P. Houdy and M. Lahmani, Nanomaterials and Nanochemistry, Springer, Berlin Heidelberg (2007)
[2]. D. V. Talapin and E. V. Shevchenko, Introduction: Nanoparticle Chemistry, Chem. Rev 116, 18, 10343 (2016)
[3]. R. Kamarudheen, G. Kumari and A. Baldi, Plasmon-driven synthesis of individual metal@semiconductor core@shell nanoparticles, Nat. comm. 11. 3957 (2020)
[4]. L. Novotny and B. Hecht, Principles of Nano-Optics, Cambridge: Cambridge University Press (2006)
[5]. R. Filter, K. Slowik, J. Straubel, F. Lederer and C. Rockstuhl, Nanoantennas for ultrabright single photon sources, Opt. Lett 39, 5, 1246 (2014)
[6]. K. R. Catchpole and A. Polman, Plasmonic solar cells, Opt. Express 16, 26, 21793 (2008)
[7]. D. Astruc, Introduction: Nanoparticles in Catalysis, Chem. Rev 120, 2, 461 (2020)
[8]. E. Cortés, W. Xie, J. Cambiasso, A. S. Jermyn, R. Sundararaman, P. Narang, S. Schlüker and S. A. Maier, Plasmonic hot electron transport drives nano-localized chemistry, Nat. Comm 8, 14880 (2017)
[9]. H. Zhang, Y-C. Liu, C. Wang, N. Zhang and C. Lu, Hybrid photonic-plasmonic nano-cavity with ultra-high Q/V, Opt. Lett 45, 17, 4794 (2020)
[10]. B. Willingham and S. Link, Energy transport in metal nanoparticle chains via sub-radiant plasmon modes, Opt. Express 19, 6450 (2011)
[11]. E. Fort and S. Grésilllon, Surface enhanced fluorescence, J. Phys. D : Appl. Phys 41, 013001 (2008)
[12]. A. Bek, R. Jansen, M. Ringler, S. Mayilo, T. A. Klar and J. Feldmann, Fluorescence Enhancement in Hot Spots of AFM-Designed Gold Nanoparticle Sandwiches, Nano Lett 8, 485 (2007)
[13]. A. Dousse, L. Lanco, J. Suffczynski, E. Semenova, A. Miard, A. Lemaıtre, I. Sagnes, C. Roblin, J. Bloch, and P. Senellart, Controlled Light-Matter Coupling for a Single Quantum Dot Embedded in a Pillar Microcavity Using Far-Field Optical Lithography, Phys. Rev. Lett 101, 267404 (2008)
[14]. P. Bharadwaj, B. Deutsch and L. Novotny, Optical Antennas, Adv. Opt. Photonics 1, 438 (2009)
[15]. M. Böhmer and J. Enderlein, Orientation imaging of single molecules by wide-field epifluorescence microscopy, J. Opt. Soc. Am. B 20, 554 (2003)
[16]. Xavier Brokmann, Marie-Virgine Ehrensperger, Jean-Pierre Hermier, Antoine Triller, Maxime Dahan, Orientational imaging and tracking of single CdSe nanocrystals by defocused microscopy, Chem. Phys. Lett 406, 1, 210 (2005)
[17]. C. Lethiec, J. Laverdant, H. Vallo, C. Javaux, B. Duvertret, J-M. Frigerio, C. Schwob, L. Coolen and A. Maître, Measurement of Three-Dimensional Dipole Orientation of a Single Fluorescent Nanoemitter by Emission Polarization Analysis, Phys. Rev. X 4, 021037 (2014)
[18]. M. A. Lieb, J. M. Zavislan and L. Novotny, Single-molecule orientations determined by direct emission pattern imaging, J. Opt. Soc. Am. 21, 6, 1210 (2004)

[19]. T. Ha, T. A. Laurence, D. S. Chemla and S. Weiss, Polarization Spectroscopy of Single Fluorescent Molecules, J. Phys. Chem. B 103, 33, 6839 (1999)
[20]. S. A. Empedocles, R. Neuhauser and M. G. Bawendi, Three-dimensional orientation measurements of symmetric single chromophores using polarization microscopy, Nature 399, 126 (1999)
[21]. L. Pelliser, M. Manceau, C. Lethiec, L. Coolen, A. Maître, A. Bramati, E. Lacaze, Controlling the alignement and orientation of single dots in rods through the use of linear defect in liquid crystal, Advanced Functionnal Materials 25, 1719 (2015)
[22]. A. Debarre, R. Jaffiol, C. julien, D. Nutarelli, A. Richard, P. Tchénio, F. Chaput and J-P. Boilot, Quantitative determination of the 3D dipole orientation of single molecules, Eur. Phys. J. D 28, 67 (2004)
[23]. Chang, W. Q.; Ha, J. W.; Slaughter, L. S.; Link, S. Plasmonic nanorod absorbed as orientation sensors. Proc.Nat.Acad.Sci. U.S.A., 107, 2781 (2010)
[24]. Ha, J. W.; Marchuk, K.; Fang, N. Focused Orientation and Position Imaging (FOPI) of Single Anisotropic Plasmonic Nanoparticles by Total Internal Reflection Scattering Microscopy. Nano Lett 12, 4282 (2012)
[25]. A. Cyphersmith, K. Early, A. Maksov, J. Graham, Y. Wang and M. Barnes, Disentangling the role of linear transition dipole in band-edge emission from single CdSe/ZnS quantum dots: Combined linear anisotropy and defocused emission pattern imaging, Appl. Phys. Lett 97, 121915 (2010)
[26]. F. Feng, L. T. Nguyen, M. Nasilowski, B. Nadal, B. Dubertret, A. Maître and L. Coolen, Probing the Fluorescence Dipoles of Single Cubic CdSe/CdS Nanoplatelets with Vertical or Horizontal Orientations, ACS Photonics 5, 5, 1994 (2018)
[27]. J. R. Navarro, D. Manchon, F. Lerouge, N. Blanchard, S. Marotte, Y. Leverrier, J. Marvel, F. Chaput, G. Micouin, A. M. Gabudean, A. Mosset, E. Cottancin, P. Baldeck, K. Kamada and S. Parola, Synthesis of PEGylated gold nanostars and bipyramids for intracellular uptake, Nanotechnology 23, 465602 (2012)
[28]. C-N. Vu, Z. Ouzit, C. Lethiec, A. Maître, L. Coolen, F. Lerouge and J. Laverdant, Single Gold Bipyramid Nanoparticle Orientation Measured by Plasmon-Resonant Scattering Polarimetry, J. Phys. Chem. Lett 12, 752 (2021)
[29]. L. Xiao, YX. Qiao, Y. He and E-S. Yeung, Three Dimensional Orientational Imaging of Nanoparticles with Darkfield Microscopy, Anal. Chem. 82, 5268 (2010)
[30]. J. Liu, A. Maitre, and L.Coolen, Tailoring Experimental Configurations to Probe Transition Dipoles of Fluorescent Nanoemitters by Polarimetry or Fourier Imaging with Enhanced Sensitivity, J.Phys.Chem.A 125, 34, 7572 (2021)
[31]. J. Liu, L. Guillemeney, A. Choux, A. Maitre, B. Abécassis, and L. Coolen, Fourier-Imaging of Single Self-Assembled CdSe Nanoplatelet Chains and Clusters Reveals out-of-Plane Dipole Contribution, ACS Photonics, 7, 10, 2825 (2020)
[32]. R. Chacon, A. Leray, J. Kim, K. Lahlil, S. Mathew, A. Bouhelier, J. Kim, T. Gacoin and G. Colas des Francs, Measuring the Magnetic Dipole Transition of Single Nanorods by Spectroscopy and Fourier Microscopy, Physical Review Applied 14, 5 (2020)